Ab initio study of structural and electronic properties of planar defects in Si and SiC

C. Raffy,* J. Furthmüller,† J.-M. Wagner, and F. Bechstedt
Institut für Festkörpertheorie und -optik, Friedrich-Schiller-Universität, Max-Wien-Platz 1, 07743 Jena, Germany
(Received 28 April 2004; published 29 November 2004)

We present *ab initio* calculations for internal interfaces in Si and SiC. Density-functional calculations within the local-density approximation and the pseudopotential-plane-wave approach are performed to understand the effect of such two-dimensional defects on the electronic properties. We study the interface between the 3*C* and 2*H* polytypes along the [111]/[0001] direction. A {221} tilt boundary between two cubic crystals, which is often observed in chemical vapor deposited films of SiC, is examined. We also consider the interface corresponding to a {115}/{$3\bar{3}02$} plane between the 3*C* and 2*H* phases. It is especially interesting since it may contribute to a quantum-wirelike inclusion of cubic SiC in hexagonal SiC. Whereas the {111}/{0001} interface induces only shallow states in the bulk fundamental gaps, the particular bond-ring topology of the {221} and {115}/{$3\bar{3}02$} interfaces gives rise to a variety of states, even resulting in a metallic behavior in the latter case for SiC.

DOI: 10.1103/PhysRevB.70.195344 PACS number(s): 61.72.Mm, 61.72.Nn, 71.55.Cn

I. INTRODUCTION

As the microelectronic devices become smaller and smaller, their performance is more and more sensitive to extended defects. The understanding of the properties of these defects in semiconductors is crucial. Among the extended defects, planar defects are of particular importance, especially stacking faults (SF's) and grain boundaries (GB's). In a crystal with stacking faults, the various lattice planes are not stacked in the same way as in the ideal crystal. The bond-stacking sequence is distorted by removal or addition of lattice planes, or certain lattice planes are rotated by an angle. A SF can be also interpreted as two nearby twin boundaries. Several kinds of SF's have been found, for instance, intrinsic, extrinsic, or twin stacking faults.[1–4] SF's are particularly important for compounds showing a pronounced polytypism such as silicon carbide (SiC).[5,6] More than 200 polytypes are known for this material. The cubic zincblende polytype 3*C* and the hexagonal polytypes *nH* ($n=2,4,6$) are the most important ones. However, extrinsic SF's have also been found in Czochralski-grown Si crystals, as well as in ion-implanted and annealed Si wafers.[7,8] They can also be induced by oxidation.[9] Because of the relationship of periodic arrangement of SF's and polytypes, boundaries between two polytypes may be considered to belong to the same type of two-dimensional defects.

Grain boundaries occur in crystals which consist of two differently oriented single crystal halves. The grain boundary is the lattice plane at which the two half crystals meet. Particularly important are the tilt boundaries, which involve a rotation about an axis in the plane of the interface. Tilt boundaries are frequently observed in chemical-vapor-deposited films of covalent materials. In particular, the so-called $\Sigma 9\{221\}$ boundary at 38.94° is common in Si and cubic SiC.[10] In this notation, the intersection of the lattices of the two fcc crystals is considered. The sites common to both lattices form a coincidence site lattice (CSL). The number 9 gives the ratio of the unit-cell volume of the CSL to that of the original lattice.[10] The {111} planes of the two crystals are at an angle of 38.94° to each other; the boundary can be thought of, therefore, as a 38.94° tilt boundary[11] around the $\langle 1\bar{1}0\rangle$ axis. Alternatively, it can be viewed as a twin boundary with a {221} plane being the twinning plane.[12] Hornstra has proposed structural models for several tilt boundaries in diamond-structure materials.[13] He has demonstrated that any tilt boundary with a $\langle 1\bar{1}0\rangle$ direction as the rotation axis can be described by an array of parallel dislocations. In materials showing polytypism, combinations of tilt boundaries and boundaries between two polytypes are also likely to occur.

Planar defects are usually regarded as causing deleterious electrical effects. In silicon, the GB's (Ref. 14) and the extrinsic SF's (Ref. 8) were shown to affect device performance by generating electronic states in the band gap, causing the segregation of impurities, or acting as electrical traps for the charge carriers. Liu *et al.* put the degradation of the electrical characteristics of bipolar SiC devices down to the stacking faults.[15] Miao *et al.* also studied the impact of the stacking faults on electronic devices and concluded on their deterioration under long time operation.[4] Iwata *et al.*[16] have shown from first-principles calculations that some SF's in 3*C*-, 4*H*-, and 6*H*-SiC can be electrically active by introducing states in the fundamental gap below the bulk conduction-band minimum. Grain boundaries may also affect the mechanical properties, by acting as initial zones of fracture with local stress concentration. Kohyama has studied the mechanical behavior of some grain boundaries in materials under stress by doing *ab initio* tests.[17]

Combinations of SF's or GB's may be used to construct homomaterial but heteropolytypical structures with interesting novel properties. Examples are homomaterial heterostructures consisting of a certain polytype with a small gap embedded in another one with a larger gap.[18,19] The problem of the lattice mismatch disappears in this kind of systems. Recently, such a layered system has been realized with thin cubic 3*C* layers embedded between thick barrier layers of the 4*H* polytype of SiC.[20–23] More complicated heterocrystalline nanostructures are conceivable. As an example, Fig. 1 presents a model of a quantum wire made up of a cubic 3*C*

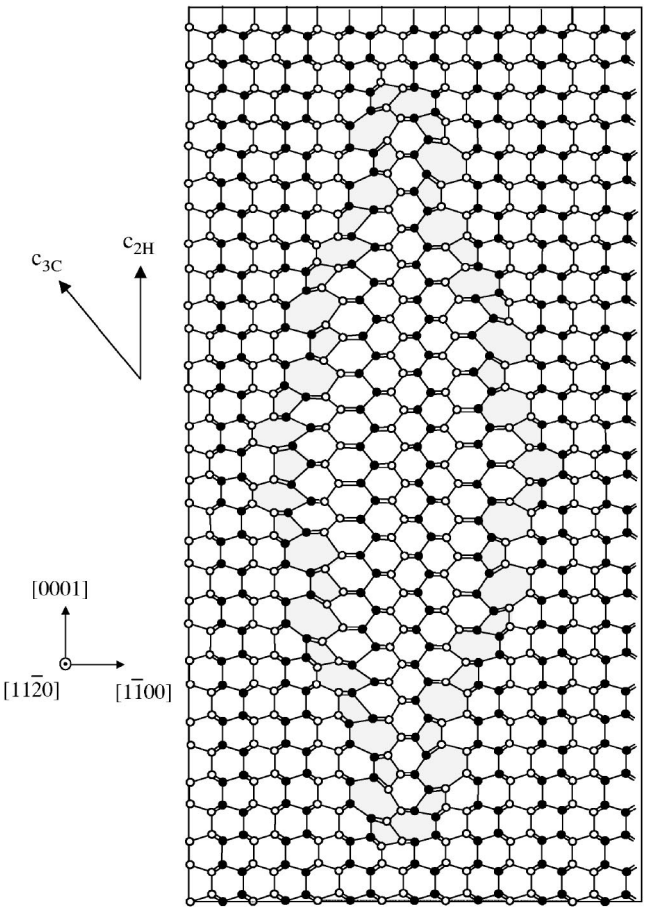

FIG. 1. Schematic model (cross section) of a quantum wire consisting of a cubic (3*C*) inclusion in a 2*H* matrix of a binary compound or a group-IV material. The atoms with the same color belong to the same $\{11\bar{2}0\}$ plane. The [111] orientation of the cubic inclusion is indicated with respect to the hexagonal *c* axis.

inclusion embedded in a hexagonal 2*H* (wurtzite) matrix. Heterostructures of this type should be observable in the SiC material. In the case of Si, the reverse configuration (2*H* embedded in 3*C*) is more interesting, since the band-gap energy decreases with hexagonality of the polytype, contrary to SiC.[3] In any case, the interfaces of such embedded quantum wires represent tilt grain boundaries between different polytypes with a complicated bonding topology.

In order to understand better the influence of planar defects on material properties, their detailed study is required on an atomic scale. The atomic structure of a number of tilt boundaries in diamond-structure crystals such as Si and Ge is reasonably well understood, using both experimental and theoretical methods. This is not the case for the electronic structure because of the limitations in the methods of investigation. An excellent overview of the relationship of the structural and electrical properties of grain boundaries in semiconductors as well as the effects of segregation and diffusion at boundaries can be found in a review article of Grovenor.[14] In this article, many studies of low- and high-angle grain boundaries are discussed. More recently, Kohyama has presented an extensive review of computational studies of tilt GB's in covalent semiconductors (Si, Ge, diamond, SiC) and in oxide semiconductors such as TiO_2 and ZnO.[10] In addition to the structural, energetical, and electronic properties, the behavior of dopants at GB's and the mechanical properties were examined. Meanwhile, a couple of first-principles studies of grain boundaries have been published. Based on density functional theory in the local density approximation and pseudopotentials, Arias and Joannopoulous[24] have performed studies of the undoped and doped $\Sigma 5\{310\}$ tilt interface in germanium. They have shown that this is a perfectly rebonded grain boundary with no dangling bonds. It introduces electron-trap states just below the conduction-band edge. Their calculations suggest that *n*-type but not *p*-type dopants segregate to the germanium boundaries. Similar studies have been done for $\Sigma 9\{221\}$ tilt boundaries in Si (Ref. 12) and in polar systems.[17] In addition, several semiempirical calculations based on the tight-binding method have been performed for grain boundaries.[11,25]

In this work, three different prototypical planar defects are studied using first-principles calculations. The aim is to determine how the interface between two crystal halves or polytypes affects the electronic properties due to both structural and chemical modifications. We proceed with increasing complexity of the interface. Each interface is studied for two materials, Si and SiC. The fact that SiC is a compound material brings an additional complexity in some cases. To keep fourfold-coordinated atoms and to avoid dangling bonds, a local nonstoichiometry may occur at the interface due to wrong Si—Si and C—C bonds. We first study the simple $\{111\}/\{0001\}$ interface between 3*C* and 2*H* polytypes, which is perpendicular to the stacking axis of the Si—Si or Si—C bilayers. Then we examine the $\Sigma 9\{221\}$ tilt boundary which was described previously. Finally, we study the interface between 3*C* and 2*H* polytypes corresponding to a $\{115\}$ or $\{3\bar{3}02\}$ plane. Such an interface occurs in the model of a homomaterial quantum wire presented in Fig. 1 Interfaces of this type have been identified experimentally in silicon[26–28] and germanium.[29] Their properties combine the characteristics of the first two types of interfaces, since they separate two crystals with tilted stacking axes and different polytypes. For the three types of planar defects, we discuss the structure, the energetics, and the electronic properties. In particular, the bonding behavior, the band structure, and the nature of electronic gap states are examined.

II. METHOD

Our calculations are based on the density-functional theory (DFT) in the local-density approximation (LDA).[30,31] The Vienna *ab initio* simulation package (VASP)[32] is used. The potential energy of an electron in the field of the nuclei screened by the core electrons is represented by nonnorm-conserving ultrasoft pseudopotentials.[33] The single-particle wave functions are expanded into a plane-wave basis set. The kinetic-energy cutoffs considered are 12.9 Ry for Si and 14.8 Ry for SiC. The electron-electron interaction is represented by the Ceperley-Alder functional as parametrized by Perdew and Zunger.[34] The **k**-space integrals, which appear in the expression of the total energy and the electron density, are replaced by sums over special points of the Brillouin

zone (BZ) generated by the Monkhorst-Pack method.[35] We use 12 special **k** points in the irreducible BZ for a {111} interface, and three for {221} and {115} boundaries. Repeated supercells are used to model planar defects, as described in the following section. Each supercell contains two planar defects, which are identical for centrosymmetric cells or represent two different boundaries in the asymmetric case.

In oder to determine the minimum-energy geometries of the defects, we allow the relaxation of all atoms within the supercell. The convergence is considered to be reached as far as the Hellmann-Feynman forces on each atom are less than 0.02 eV/Å. We do not take into account a possible expansion of the material due to the presence of planar defects. Consequently, the total volume is kept fixed. Variations of the GB thicknesses are assumed to be negligible in comparison with the vertical extent of the supercells.

For the representation of the interface or defect states, we assume that the BZ of the used supercell system is flat. The band dispersion perpendicular to the interface is negligible. The supercell bands are plotted versus wave vectors along high-symmetry lines in the resulting two-dimensional BZ. In order to figure out the localization of these states, their energies are compared with the bulk band structure projected onto the two-dimensional BZ.[36] The alignment of the band energy levels between the configuration with interface and the configuration without boundaries is done using the electrostatic potential. The electrostatic potential is derived from the local part of the pseudopotentials, the Hartree potential, and the exchange-correlation potential, i.e., it is the local single-particle potential in the Kohn-Sham equation.

In order to discuss the energetics and the stability of the planar defects, we calculate formation energies. The average formation energy E_f of one interface per unit cell (or γ_f per unit area) follows as the difference of the total energy of the supercell and the total energies of the ideal crystals bounded by two interfaces

$$2E_f = E_{\text{supercell}} - (n_1E_1 + n_2E_2), \tag{1}$$

where n_1 and n_2 are the numbers of atoms in the parts 1 and 2 of the supercell, respectively, and E_1 and E_2 are the corresponding energies per atom. In our case, according to the respective interface under study, 1 and 2 represent either 2*H* and 3*C* or 3*C* and tilted 3*C*.

In the case of two different polytypes in a supercell, i.e., a superlattice of two polytypes with corresponding interfaces, additionally an energy E_{in} (polytype) is introduced. It defines the energy required to insert layers of a certain polytype in a matrix consisting of layers of another polytype:

$$E_{\text{in}}(2H) = E_{\text{supercell}} - nE_{3C}, \tag{2a}$$

$$E_{\text{in}}(3C) = E_{\text{supercell}} - nE_{2H}, \tag{2b}$$

where n is the total number of atoms in the supercell.

III. RESULTS AND DISCUSSION

A. The {111}/{0001} 3*C*/2*H* interface

This interface represents the transition between a cubic (diamond or zinc blende) crystal and a hexagonal (wurtzite) crystal along the stacking direction. The hexagonal stacking can be achieved by the shear of $\frac{1}{6}[112]$ partial dislocations on every other {111} plane of an original fcc crystal.[27] This mechanism changes the stacking sequence from *ABCABC* to *ABABAB*. The stacking direction is $[111]_{\text{cub}} \| [0001]_{\text{hex}}$. The two other equivalent orientations in the cubic and hexagonal modifications are $[11\bar{2}]_{\text{cub}} \| [1\bar{1}00]_{\text{hex}}$ and $[1\bar{1}0]_{\text{cub}} \| [11\bar{2}0]_{\text{hex}}$ (see Fig. 2). Such interfaces can indeed occur in Si crystals. Layered inclusions of the 2*H* wurtzite phase have been observed in Si samples under high pressure (Ref. 3, and references therein). In the case of the compound SiC, this inter-

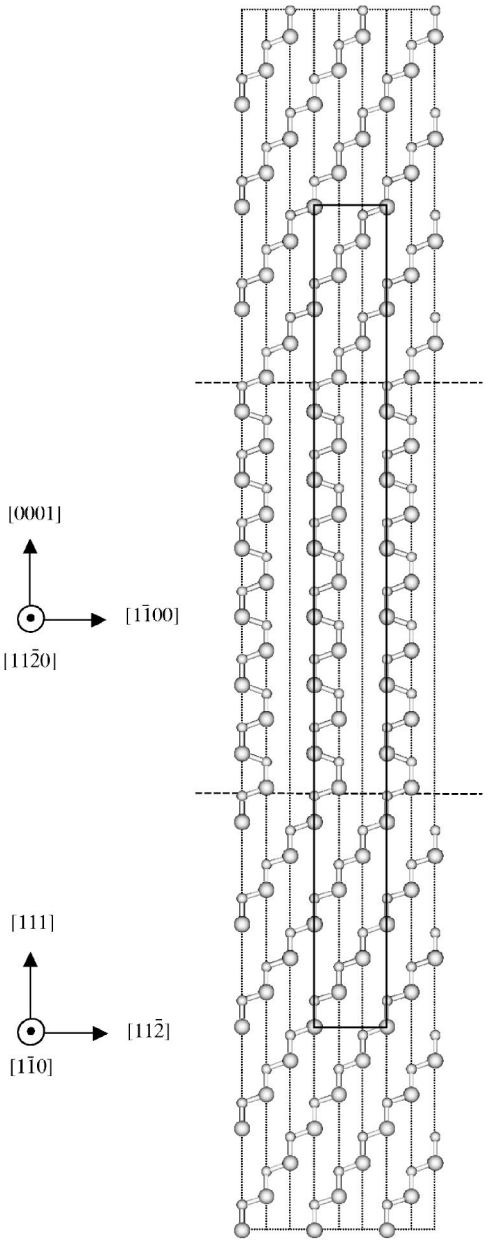

FIG. 2. A cross section of the {111}/{0001} interface between 3*C*- and 2*H*-SiC. More strictly, a projection onto a $\{1\bar{1}0\}$ or $\{11\bar{2}0\}$ plane is plotted. The supercell used is indicated by solid lines. The lattice vectors of the resulting hexagonal Bravais lattice are $\mathbf{a}_1$, $\mathbf{a}_2$, and $\mathbf{c}$, with the hexagonal lattice constants $a = 3.055$ Å and $c = 59.868$ Å. The interfaces are indicated by dashed lines.

TABLE I. Energetics of {111}/{0001} and {115}/{$3\bar{3}02$} interfaces between cubic and hexagonal Si. The values for SiC are given in parentheses.

	{111}/{0001}	{115}/{$3\bar{3}02$}
E_f (meV/interface atom)	−11.0 (−0.6)	37 (305)
γ_f (mJ/m^2)	−13.9 (−1.1)	188 (2420)
$E_{\text{in}}(2H)$ (meV/atom)	5.1 (0.9)	13.6 (68.4)
$E_{\text{in}}(3C)$ (meV/atom)	6.0 (−0.9)	2.5 (66.9)

face represents an exemplary system, since the wurtzite phase of SiC is very rare. Combinations with the more common 4*H* and 6*H* structures are more likely. The heterocrystalline transition 3*C*/2*H* is therefore studied as a model interface.

The {111}/{0001} interface is modelled by an arrangement of supercells represented in Fig. 2 for the SiC case. A supercell consists of 24 Si—Si or Si—C bilayers. The periodically continued structure corresponds to a superlattice denoted with $(3C)_4(2H)_6$,[37] where the index gives the number of primitive unit cells of the indicated polytype in stacking direction. The system is slightly strained. Indeed, the lateral lattice constant a and the height of the bilayers h are taken as the ideal values calculated for the 3*C* polytype (a = 3.816 Å and h = 3.115 Å for Si, a = 3.055 Å and h = 2.494 Å for SiC). However, the strain effects are negligible. Each supercell contains two interfaces. They are equivalent in the case Si, since one is the image of the other due to inversion symmetry. In contrast, they are inequivalent in the case of SiC, due to the polarity of the compound. We mention that the distance between the interfaces (37.4 Å for Si, 30.0 Å for SiC) is large enough to guarantee an almost vanishing interaction between each other.

After the total-energy optimization, we observe that the changes in the atomic positions are negligibly small. This is a consequence of the structural similarities between the cubic and hexagonal bilayers. The calculated interface energies in Si and SiC are listed in Table I. The negative values indicate that the creation of such twinning interfaces is seemingly energetically favorable. For SiC this is not surprising, since the periodic arrangement of cubic and hexagonal bilayers found for the 4*H* polytype is known to be the energetically most favorable structure. The interpretation for Si must take into account the fact that we compare the energy of the interface system with the energy of the isolated materials with a purely cubic or purely hexagonal stacking, see Eq. (1). For Si, the 2*H* polytype is completely unfavorable,[3] which explains why we find a large energy gain for the interface formation. In the case of SiC, however, there is only a tiny energy difference between the 2*H* and the 3*C* polytype.[38] Therefore, a lower energy gain is obtained. Actually, the negative value of E_f simply means that it is energetically more favorable to have a "mixed" 2*H*/3*C* system rather than two separated grains of 2*H* and 3*C*. We mention that the interface energy is very sensitive to the size of the supercell. In a previous calculation with only a twelve-bilayer SiC supercell,[39] we found −3.0 meV/interface atom (−5.9 mJ/m^2), instead of −0.57 meV/interface atom (−1.1 mJ/m^2). The larger absolute values for smaller supercells are a consequence of the particle-in-a-box effect.

The quantity that reflects more the energetics of the bulk polytypes is the energy of insertion, see Eq. (2). The calculated energies for inserting 2*H* in 3*C* or 3*C* in 2*H* are respectively positive and negative, in agreement with the fact that the 2*H* polytype is less stable than the 3*C* polytype in both cases, Si and SiC.[3,38] Again, we observe a different result compared to the calculation using a twelve-bilayer SiC supercell.[39] However, the difference, which is only approximately 0.25 meV/atom (absolute value), is close to the energy resolution of our method and can be considered negligible.

The electronic properties of the heteropolytypic superlattice system are governed by the single-particle potential in the Kohn-Sham equation of the DFT-LDA. Figure 3 shows the variation of the local electrostatic potential along the direction perpendicular to the interface in the case of SiC. The

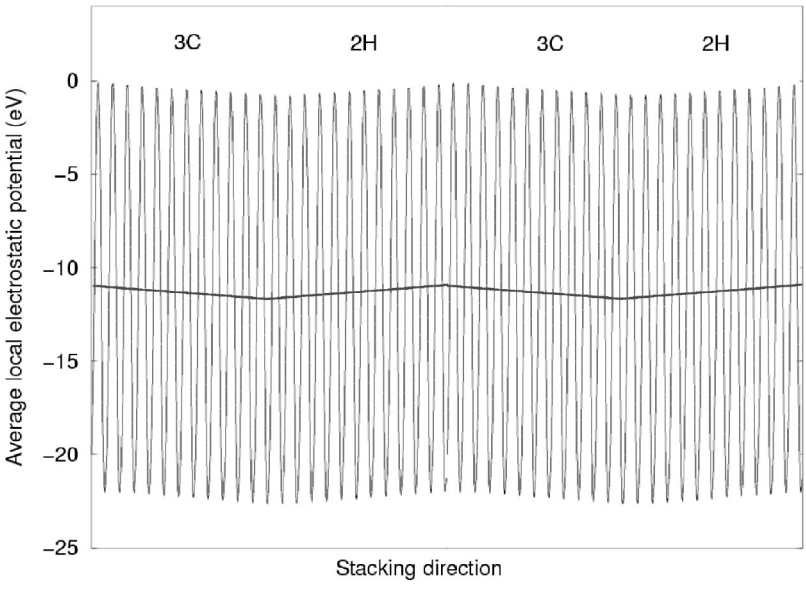

FIG. 3. Plane-averaged electrostatic potential along the normal direction of the {111}/{0001} SiC interface. The spatial variation of the maxima/minima is indicated by the thick solid line.

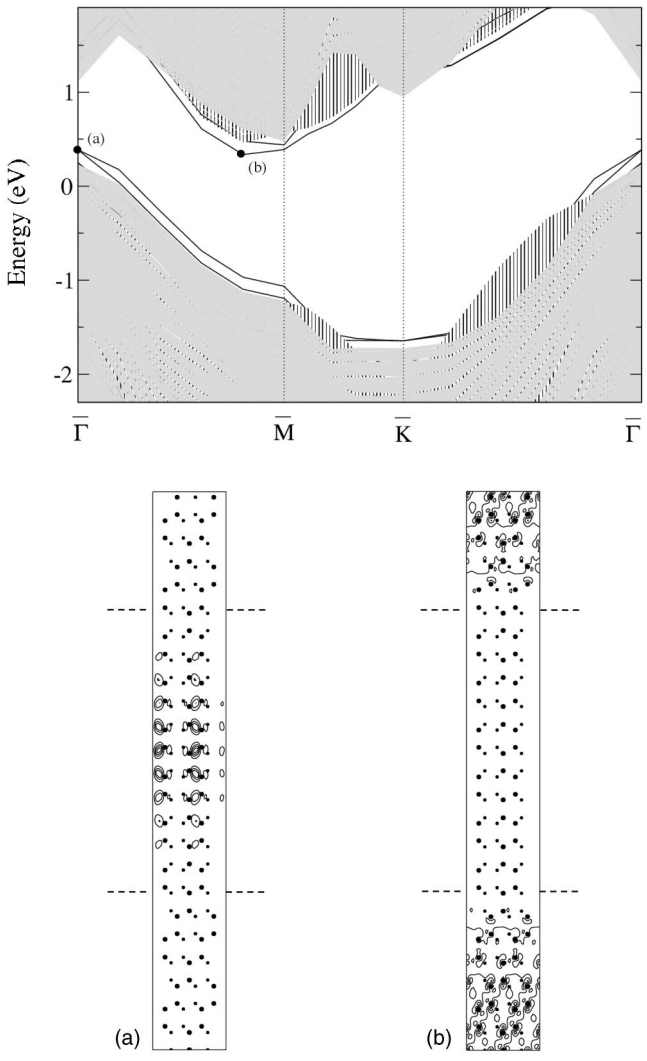

FIG. 4. Electronic band structure of the {111}/{0001} Si interface (upper panel). The projections of the 3*C*- and 2*H*-bulk bands are hatched and shaded, respectively. The wave-function squares of the highest occupied state (a) and the lowest empty state (b) are plotted within one supercell (lower panel).

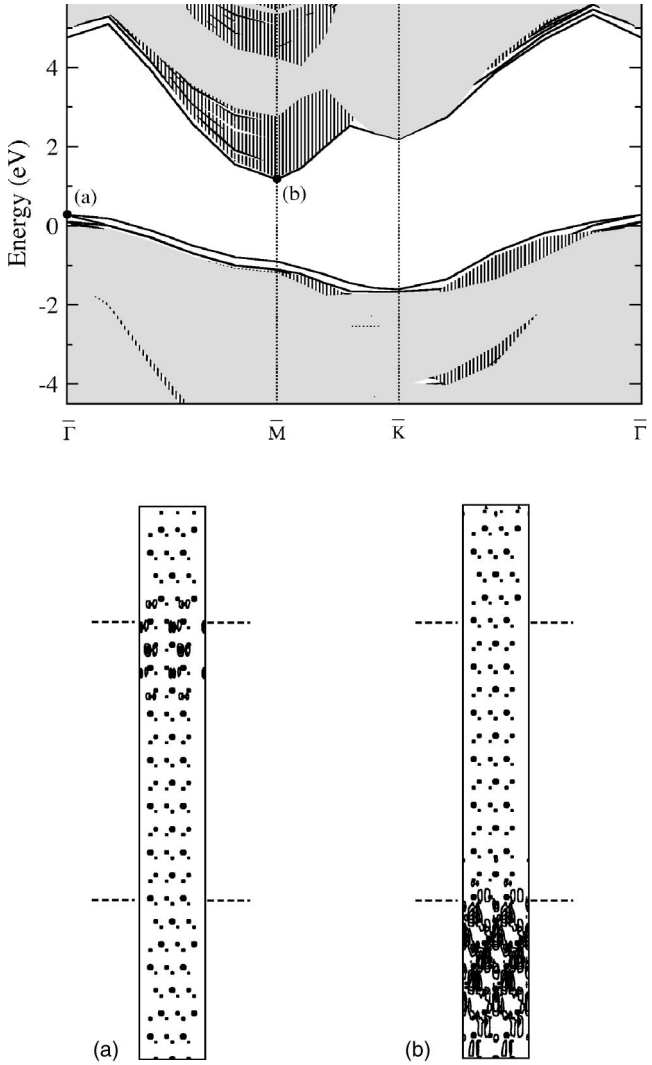

FIG. 5. Electronic band structure of the {111}/{0001} SiC interface. Same legend as in Fig. 4.

average values of the potential in each plane parallel to the interface are reported. The oscillations of this potential along the stacking direction are clearly visible. The envelope of the electrostatic potential shows a saw-tooth shape due to the spontaneous polarization created by the dipoles between the nonequivalent bonds in the 2*H*-SiC crystal. The effect of the spontaneous polarization in 2*H* becomes visible due to the presence of the interfaces. As a consequence of the electrostatic boundary conditions, electric fields with different signs appear in the layers with different bond stackings between the interfaces. For SiC, the calculated internal macroscopic electric fields have the same absolute value in the 3*C* and 2*H* parts (which have the same thickness): $F_{3C}=F_{2H}=2.3$ MV/cm. The corresponding macroscopic potential in Fig. 3 exhibits minima and maxima at the interfaces.

The resulting electronic properties are represented in Figs. 4 and 5 for Si and SiC. The band structures of the interfaces are shown in the upper panels, together with the projection of the allowed 3*C*- and 2*H*-bulk states onto the hexagonal interface Brillouin zone (hatched and shaded regions). For both Si and SiC, the band structures reveal only shallow interface states above the bulk valence band maximum (VBM) and below the bulk conduction band minimum (CBM). The projected fundamental gaps of both 3*C*- and 2*H*-band structures are otherwise almost free of states induced by the interfaces. In order to understand the nature of these shallow states, corresponding wave-function squares are plotted in the lower panels. Figures 4(a) and 5(a) represent the wave-function squares of the highest occupied states at $\bar{\Gamma}$, for Si and SiC. In both cases, the wave function is localized in the 2*H* region. However, in the case of SiC, the state is localized near one interface. The wave function extends more at the 2*H* side with a strong decay into the 3*C* region. Figures 4(b) and 5(b) represent the wave-function squares of the lowest unoccupied states near $\bar{M}$ and at $\bar{M}$, for Si and SiC, respectively. In both cases, the wave function is localized in the 3*C* part. In the case of SiC, the state is again localized near one interface. These results can be explained by the type-II hetero-

structure character of the $(3C)_4(2H)_6$ superlattices in Si and SiC, together with the electrostatics in the case of SiC. The holes should be confined in the hexagonal region, whereas the electrons should be confined in the cubic part.

In the case of Si, the type-II character found here is in contradiction with previous calculations[3] on the isolated polytypes. The calculations gave a valence-band discontinuity of $\Delta E_v = -0.235$ eV and a conduction-band discontinuity of $\Delta E_c = -0.035$ eV, which indicated a type-I heterostructure. Tight-binding calculations of Murayama *et al.*[40] also indicate a type-I character. The disagreement is due to the fact that the band gap of cubic Si calculated in the previous work (0.54 eV[3]) is not the minimum gap. The calculation was done considering the hexagonal BZ. But the true CBM, which occurs on the ΓX line in the fcc representation, is not located on the hexagonal high-symmetry lines. The proper minimum gap is 0.46 eV,[41] which gives a conduction-band discontinuity of +0.045 eV, i.e., a type-II character in agreement with the present results. A very accurate determination of the conduction-band minimum position in **k** space is required in order to obtain sufficiently accurate minimum gap values to predict the type-I or type-II behavior correctly. Small inaccuracies in the fundamental gap values (a few ten meV) can already change the sign of the conduction-band discontinuity. In addition, we have to mention that we did other calculations by considering a noncentrosymmetric supercell (not presented). Then, the state denoted (b) is found to be localized in the 2*H* region. The ambiguity raised by these different results is due to the extremely small conduction-band discontinuity between 2*H*- and 3*C*-Si which does not generate clear quantum wells for the electrons. The results can even change according to the way the interfaces are constructed. One cannot clearly conclude about the confinement region of the electrons in the $(3C)_4(2H)_6$ Si superlattice.

In the case of SiC, the situation is more clear. The results are in agreement with the calculated band discontinuities $\Delta E_c = 0.99$ eV and $\Delta E_v = -0.13$ eV (Ref. 42) which indicate that the lowest energy electron wave functions should be localized in the 3*C* region, whereas the probability to find a hole should be larger in the 2*H* region. This picture based on the spatial variation of the band edges, CBM and VBM, is interfered by the electric-field influence accompanying the spontaneous polarization in the hexagonal crystals. The corresponding saw-tooth potential represented in Fig. 3 explains why particles with different signs of charge are localized near different interfaces. The saw-tooth potential induces spatially separated triangularlike quantum wells for electrons and holes, as indicated in Fig. 6.

The study of the interface arrangement in a superlattice also allows the interpretation of the electronic states of two other defect structures, at least in the case of SiC. The results described above are useful for the discussion of thin inclusions of 3*C* layers in a hexagonal 2*H* (or even 4*H*) matrix. Then, instead of the hatched conduction-band region of the projected 3*C* electronic states around $\bar{M}$ in Fig. 5, two-dimensional subbands appear. They are related to the fact that a 3*C* layer embedded in a hexagonal matrix forms a deep quantum well for the movement of the electrons.[20–22,43]

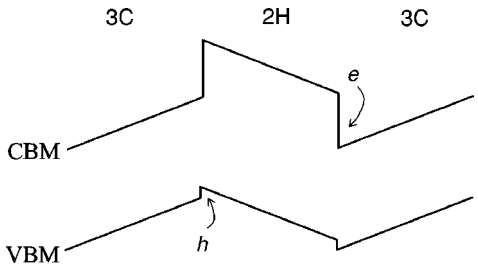

FIG. 6. Schematic band-line up for a $(3C)_4(2H)_6$ superlattice along the [111]/[0001] direction in the case of SiC. The spontaneous polarization in the hexagonal crystal is taken into account.

Another defect structure follows if the two boundaries come close to each other. Then a stacking fault appears in a cubic or hexagonal matrix. The above electronic-structure results suggest that a SF in a hexagonal crystal should be electrically active by generating efficient traps for conduction-band electrons.[4,16,43]

B. The tilted {221} interface in 3*C* crystals

The $\Sigma 9\{221\}$ tilt boundary has been the object of a number of experimental studies in Si and Ge.[7,8,44,45] High-resolution transmission electron microscopy (HRTEM) has been used to suggest atomic models. Two structures have been proposed in literature for the reconstruction at the $\{221\}$ boundary between two tilted crystal halves.[12,17] One with a glide-plane symmetry has a zig-zag sequence of five- and seven-membered rings, whereas the mirror-symmetry interface contains a linear sequence of five-, six-, and seven-membered rings. For covalent Si and Ge semiconductors, the glide-plane model has been found to be more stable than the mirror-plane model, both experimentally[44,45] and theoretically.[12] We study the glide-plane model in detail. The corresponding supercell with $[22\bar{1}]$ orientation is represented in Fig. 7. The tilt angle between the [111] orientations of the two cubic grains is $\theta = \arccos(7/9)$, i.e., 38.94°. The supercell contains 144 atoms arranged in a simple orthorhombic lattice. The extensions of the supercell have been determined from the values of the lattice parameter *a* and of the bilayer height *h*, as calculated from the elementary cell of the bulk 3*C* polytype ($a = 3.816$ Å and $h = 3.115$ Å for Si, $a = 3.055$ Å and $h = 2.494$ Å for SiC). The lattice constant in the direction perpendicular to the interfaces is 64.7 Å for Si and 51.8 Å for SiC, which guarantees that the mutual interaction of the tilt boundaries is weak.

Each supercell contains two interfaces consisting of five- and seven-membered rings. This reconstruction is similar to the π-bonded chain model of the 2×1 reconstructed Si and Ge(111) surfaces.[46,47] It is also found in the ST-12 complex crystal phase of germanium.[48] The odd-membered ring structure allows to preserve the fourfold coordination, resulting in no dangling bonds at the interfaces. However, in the case of SiC, the boundaries are characterized by nonstoichiometric numbers of cations and anions. Wrong Si—Si and C—C bonds occur, giving rise to one Si-rich and one C-rich interface. Because of the electron transfer from Si to C atoms in SiC, the Si-rich (C-rich) interface is called *p*-polar (*n*-polar).

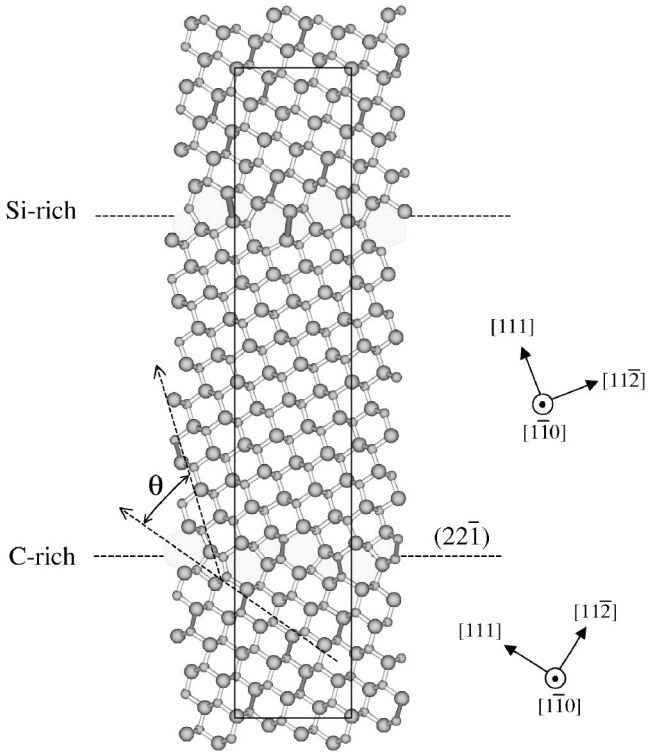

FIG. 7. A cross section of {221} interfaces in 3*C*-SiC. The supercell used is represented by solid lines. The vectors of the simple orthorhombic lattice are $\mathbf{a}_1$, $\mathbf{a}_2$, $\mathbf{a}_3$, with lattice constants $|\mathbf{a}_1|=3.055$ Å, $|\mathbf{a}_2|=9.165$ Å, and $|\mathbf{a}_3|=51.848$ Å. The tilt angle is $\theta=38.94°$.

Each planar unit cell in an interface intersects two Si—Si or C—C bonds. We mention that one may also construct nonpolar interfaces which contain both kinds of wrong bonds. Such nonpolar interfaces have been observed by HRTEM in SiC films prepared by chemical vapor deposition (CVD).[17,49] However, they should be slightly less stable than the polar ones.[17]

The arrangement of the bonds in the odd-membered rings induces some stretching or bending of the bonds, resulting locally in a certain amount of strain. Table II indicates large angular deviations from the perfect tetrahedral angle of 109.47°. For Si, the deviations vary from −16.2° to +23.1°, which is very similar to the values calculated by Kohyama.[25] Rather small bond-length variations are found. Compared with bulk Si, the Si—Si bond-length deviation only varies from −2.1 to +1.4 %. For SiC, the calculated distortions are again in very good agreement with those published in literature.[17,49] At the *p*-polar interface, the Si—Si wrong bonds have lengths rather similar to those in bulk Si, with a deviation of about −1.5%. At the *n*-polar interface, the C—C bonds show larger deviations of about +5.6% compared with bulk diamond.

TABLE III. Formation energy of the {221} grain boundary in Si and SiC. The first number gives the energy γ_f in mJ/m^2. The number in parentheses gives the energy E_f in meV per interface atom.

	Si	SiC
present	243 (41.4)	1602 (175)
other	290[a]	1240[d]
calculations	320[b]	
	320 (53.1)[c]	

[a]Reference 12.
[b]Reference 25.
[c]Reference 11.
[d]Reference 17.

The results for formation energies of {221} grain boundaries are listed in Table III. For Si, the calculated value 0.243 J/m^2 compares very well with that obtained by DiVincenzo *et al.*[12] from DFT-LDA with a local-orbital basis set and norm-conserving pseudopotentials. The average interface energy in the case of SiC amounts to $\gamma_f=1.60$ J/m^2, which is also very close to values calculated by other authors.[17,49] The positive values indicate that the formation of such complicated interfaces requires some energy to generate the change of the bonding topology. This is especially true in the case of SiC, where compressed Si—Si and stretched C—C bonds have to be created. We mention that

TABLE II. Bond-length and bond-angle distortions in a {221} grain boundary in Si and SiC. The deviations are calculated with respect to the corresponding bulk quantities. The numbers in parentheses are values from the literature.

	Si	SiC	
		n-type	*p*-type
Si—C bond		−2.8% to +1.9%	−2.2% to +3.1%
		(−2.7% to +2.0%[b])	(−2.7% to +2.5%[b])
Si—Si bond	−2.1% to +1.4%		−1.5%
	(−1.6% to +1.5%[a])		(−1.1%)[b]
C—C bond		+5.6%	
		(+4.5%[b])	
Bond angle	−16.2° to +23.1°	−20.1° to +22.8°	−13.8° to +23.7°
	(−16.2° to +20.8°[a])	(−20.1° to +22.5°[b])	(−13.0° to +24.0°[b])

[a]Reference 25.
[b]Reference 17.

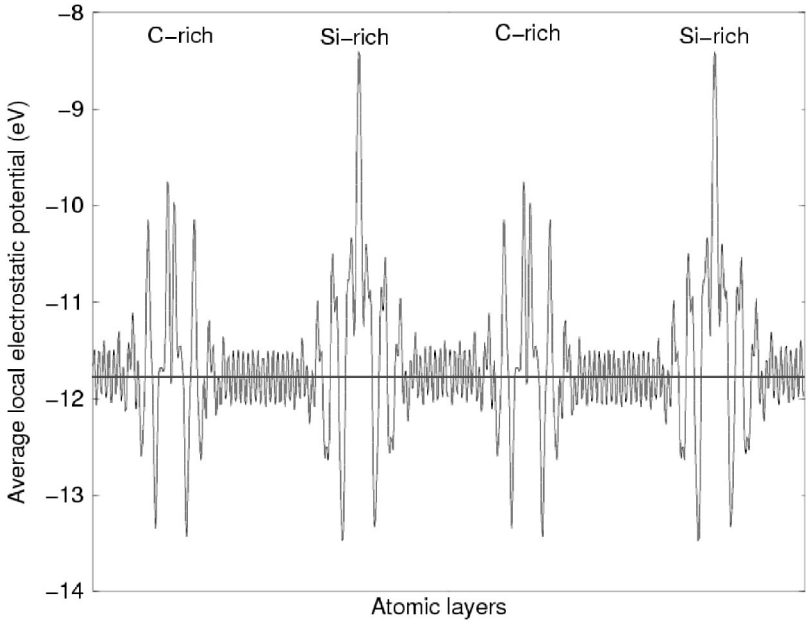

FIG. 8. Electrostatic potential along the direction perpendicular to the {221} boundaries in SiC. Two supercells are shown.

the values are much lower than the energies obtained for the free surfaces, because of the absence of dangling bonds. For example, the energy of the $(111)2\times1$ reconstructed surface of Si is about 1.45 J/m^2 (Ref. 47).

The formation energy of the tilt boundary in SiC converts to 0.175 eV per interface atom. This value approaches the thermal energy $k_BT=0.15$ eV corresponding to the substrate temperature of about 1700 K in a CVD process, and is much smaller than the thermal energy $k_BT=0.22$ eV provided during bulk growth at about 2500 K using a modified Lely method. The low formation energy may explain why {221} tilt boundaries are observed in polycrystalline SiC (Ref. 10) and even the occurrence of similar boundaries in hexagonal SiC.[50] In Si, the small value of the formation energy (0.041 eV per interface atom) also makes the generation of such two-dimensional defects likely for high temperatures, for instance, during growth processes.

A very interesting quantity to characterize the property changes due to the presence of a grain boundary is again the electrostatic potential perpendicular to the interfaces. It is plotted in Fig. 8 for SiC. Compared to the {111}/{0001} interface, a strong perturbation is observed. The variation of the potential with the atomic layers is dramatically increased in the interface regions. However, no macroscopic electric field appears between two interfaces, due to the glide-plane symmetry between the two cubic crystals.

The electronic band structures of the considered grain boundaries are presented in Figs. 9 and 10 versus high-symmetry lines in the two-dimensional rectangular BZ. In spite of the absence of dangling bonds at the grain boundary, one observes shallow states above the VBM and below the CBM for Si (Fig. 9). Compared to DiVincenzo *et al.*,[12] we found a higher density of states close to the valence bands. The nature and localization of these gap states is represented in the lower panel of Fig. 9. We have used a noncentrosymmetric supercell, so that nearly degenerate states possess wave functions in spatially different regions. The contour plots indicate that the lowest unoccupied state at $\bar{\Gamma}$ [denoted by (b)] is localized at the interface. The situation is less clear for the state above the VBM which seems to belong to the interface, although it also extends into one grain [state denoted by (a)]. We mention that we have also done calculations using a centrosymmetric supercell with a π rotation center making the two interfaces equivalent. We found the same band structure. However, the wave-function squares are more difficult to interprete due to the mixing of the states from both interfaces.

The occurrence of interface states is somehow in contradiction with other results from literature. The calculations of Thomson *et al.*[11] and of Kohyama *et al.*[10,25] did not reveal any states falling in the bulk band gap. Also, the measurements by Cunningham *et al.*[51] did not detect carrier traps at the grain boundary. The effects of the special ring topology have been studied by Joannopoulos and Cohen[52] for silicon and germanium. They have shown that odd-membered rings of atoms give rise to states in the pseudogap below the bulk valence-band maximum. Our experience indicates that the discussion of the electronic boundary states needs large supercells, inclusion of atomic relaxation in the interfaces, and precise alignment with the projected bulk band structure by using the electrostatic potentials in an appropriate direction.

For SiC the interface states accompanying the two {221} tilt boundaries are shown in Fig. 10. Occupied interface states occur in the lower part of the fundamental gap close to the VBM. The state at the $\bar{\Gamma}$ point [denoted by (a)] being 0.2 eV above the VBM is localized at the C-rich boundary at Si—C bonds of the fivefold rings, as indicated by the corresponding wave-function square. In contrast, the uppermost interface state at $\bar{M}$ is localized at the Si—Si bonds of the Si-rich boundary. In pure or *n*-doped SiC, these filled interface states should not drastically influence the electronic properties. However, their presence may reduce the *p*-doping efficiency. Shallow acceptors with levels only slightly above the VBM (<0.4 eV) may be passivated by electronic states of the tilt boundaries. An example could be the doping by aluminum atoms, which creates energy levels about 0.24 eV above the VBM in the 6*H* polytype.[53]

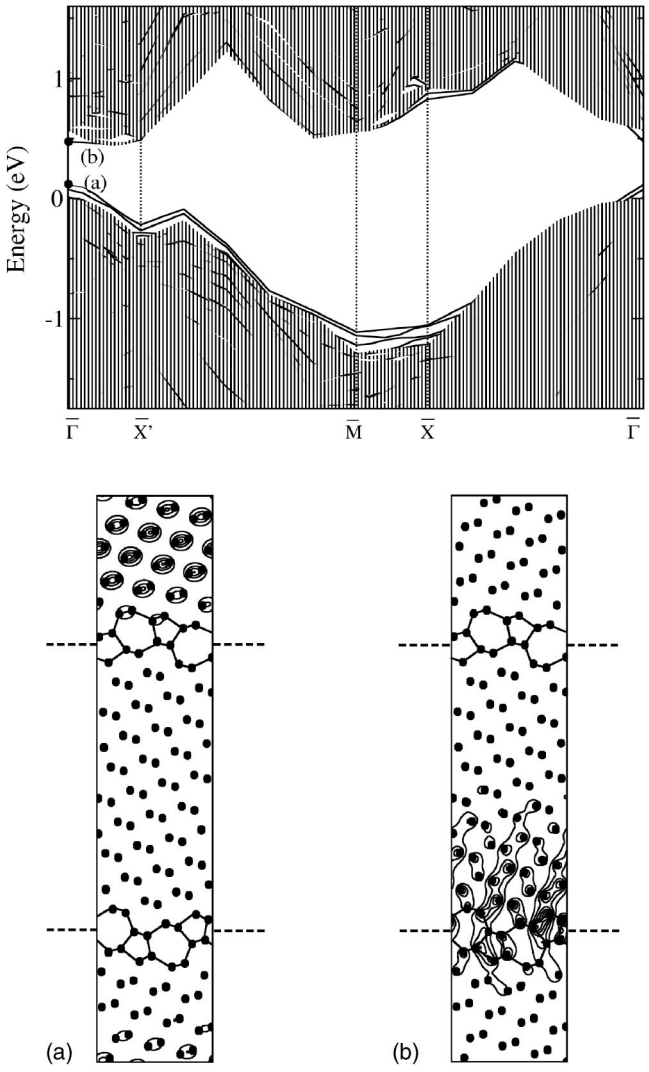

FIG. 9. Electronic band structure of a {221} grain boundary in Si (upper panel). The wave-function squares of the gap states at $\bar{\Gamma}$ are also plotted (lower panel).

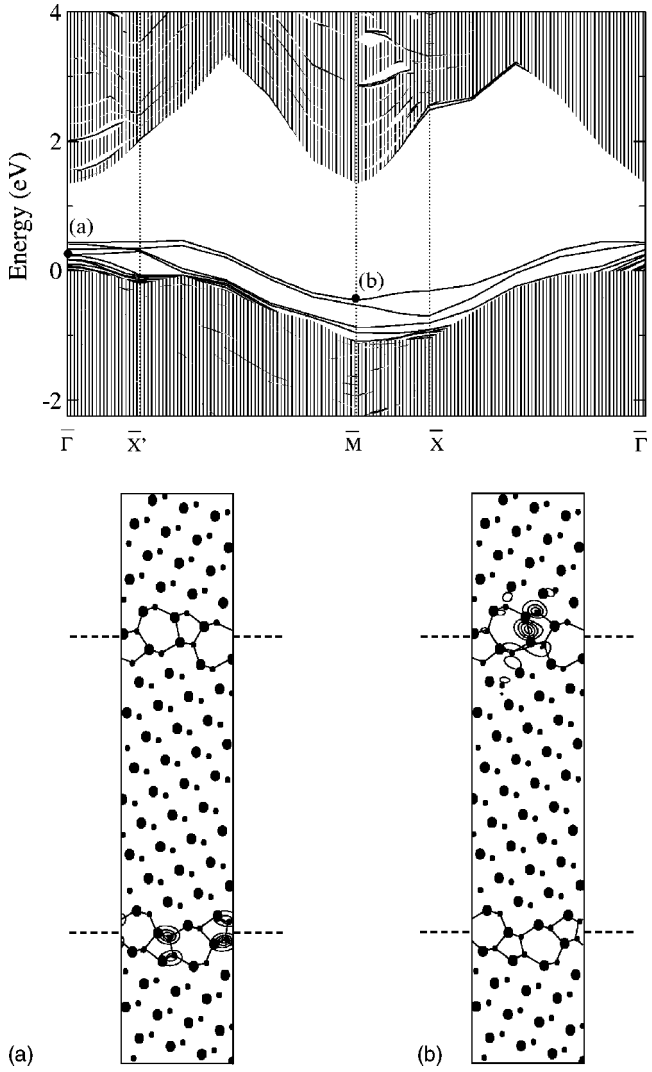

FIG. 10. Electronic band structure of Si-rich and C-rich {221} grain boundaries in SiC (upper panel). The wave-function squares of the gap states at $\bar{\Gamma}$ and $\bar{M}$ are also plotted (lower panel).

C. The tilted {115}/{$\bar{3}302$} 3*C*/2*H* interface

The change of polytype from the 3*C* to the 2*H* structure usually happens along the stacking direction [111]/[0001]. The resulting boundary has been discussed in Sec. III A. However, such a transition may also occur in other directions in space. One example is a tilted boundary of the {115} type, which coincides with a hexagonal {$\bar{3}302$} plane. Again the tilt angle is 38.94°. Experimentally, ribbons of wurtzite silicon[27,28] and germanium[29] with such an orientation have been produced in a cubic matrix after hardness indentation. The mechanism of the transformation from the cubic to the hexagonal diamond structure is analyzed accurately in terms of dislocations in various papers of Pirouz *et al.*[27–29] One model for the formation of 2*H* silicon in ion-implanted silicon wafers has been proposed by Tan *et al.*[26]

Because of the tilt angle the structure of the {115}/{$\bar{3}302$} interface is quite similar to that of the {221} interface between two cubic crystal halves. It is characterized by the occurrence of five- and seven-membered rings which allow us to keep the tetrahedral coordination. The supercell used for modeling (see Fig. 11) is composed of 216 atoms arranged in an orthorhombic lattice, with 112 atoms belonging to the cubic crystal and 104 atoms belonging to the hexagonal crystal. The dimensions of the lattice vectors are determined in the same way as for the {221} interface. The length of the supercell in the direction perpendicular to the interface is 56.1 Å for Si, and 44.9 Å for SiC.

Important geometrical parameters of the interface rings are reported in Table IV. They indicate much stronger bond-length distortions in comparison with the {221} boundaries. This is especially true for SiC, where the C—C bonds are stretched by almost 15% with respect to bulk diamond. The deviations of the bond angles from the ideal tetrahedron value are similar to those found for {221} boundaries.

The characteristic interface energies are also listed in Table I. The energy for inserting a 2*H* (3*C*) crystal in a 3*C* (2*H*) matrix with a tilt angle of 38.94° was also calculated. The values are positive and much larger than for the

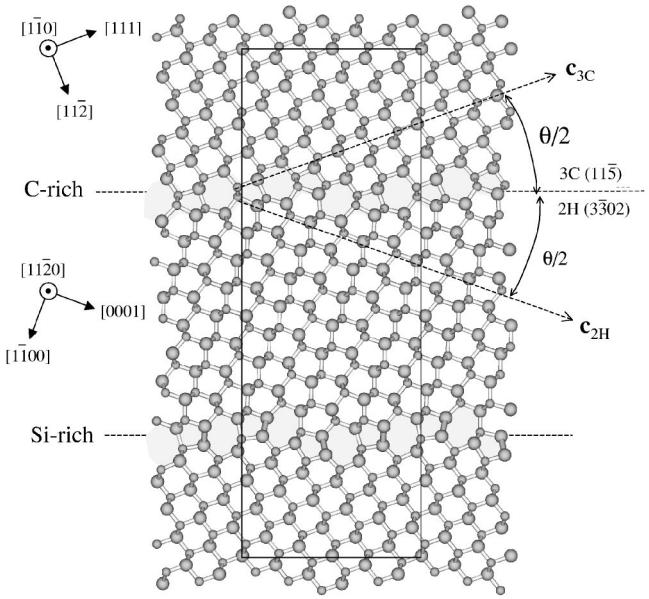

FIG. 11. A cross section of a {115}/{$\bar{3}$302} interface between 3*C*- and 2*H*-SiC. The supercell used is represented by solid lines. The vectors of the simple orthorhombic lattice are $\mathbf{a}_1$, $\mathbf{a}_2$, $\mathbf{a}_3$, with $|\mathbf{a}_1|=3.055$ Å, $|\mathbf{a}_2|=15.875$ Å, and $|\mathbf{a}_3|=44.901$ Å. The tilt angle is $\theta=38.94°$.

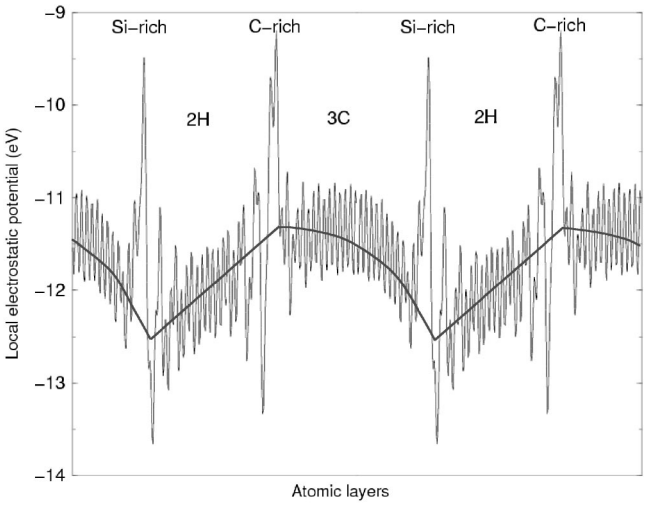

FIG. 12. Electrostatic potential along the direction perpendicular to the {115}/{$\bar{3}$302} interface in SiC. The solid line gives the potential averaged over at least two atomic layers. Two supercells are shown.

{111}/{0001} interface, especially for SiC. The positive value of $E_{\text{in}}(3C)$ indicates that the lower energy of the 3*C* phase does not compensate the energy needed to generate the distorted rings. However, in the case of Si, the formation energy of the interface is quite small, which is consistent with its occurrence in plastic zones during hardness indentation.[27,28] For SiC the calculated formation energy is 0.31 eV/interface atom. Although this is larger than the thermal energy k_BT being relevant in growth processes, the value is not too high to rule out the possibility of formation of such interfaces under growth conditions. Moreover, we have to keep in mind that 2*H*-SiC is not the most stable hexagonal polytype. It is likely that the interface energy would be lower if the 2*H* crystal is replaced by 4*H* or 6*H*.

The combination of cubic and hexagonal crystals is influenced by the presence of the spontaneous polarization in the hexagonal material. The resulting electric fields in the different polytypes can again directly be determined from the electrostatic potential represented in Fig. 12. There is a complication in the 3*C* case, since the field is not homogeneous. Only an averaged value is considered. The calculated absolute values of the fields in 2*H* and 3*C* crystals are, respectively, $F_{2H}=5.4$ MV/cm and $F_{3C}=4.5$ MV/cm. The increase of the fields with respect to the {111}/{0001} case is a consequence of the stronger perturbations by the interface with five- and seven-membered rings instead of six-membered rings.

The band structures are represented in Figs. 13 and 14. Drastic differences between the {115}/{$\bar{3}$302} interfaces in Si and SiC are obvious. For Si, only a few electronic states appear slightly above the VBM, which are well localized at interfaces. This is especially true for the gap states at the Brillouin zone boundary at $\bar{X}$. The state at Γ just above the VBM has a more bulklike character, but only occurs in the hexagonal parts of the system.

For SiC the situation is very different. Many more interface states are generated in the projected bulk gaps, even resulting in a metallic behavior. The metallic character is governed by band dispersion in the [11$\bar{2}$0] or [1$\bar{1}$0] direction. The occurrence of so many midgap states with strong dispersion is mainly due to the wrong Si—Si bonds [states (b) and (c) in Fig. 14]. Consequently, a {115}/{$\bar{3}$302} interface in SiC should have a significant effect on the electric properties, in so far as it locally destroys the semiconducting behavior of the material. As a result, we predict that the

TABLE IV. Bond-length and bond-angle distortions in the {115}/{3302} grain boundary in Si and SiC. The deviations are calculated with respect to the bulk cubic diamond or zinc blende material.

	Si	SiC	
		n-type	*p*-type
Si—C bond		−3.4% to +4.0%	−5.1% to +1.71%
Si—Si bond	−2.6% to +2.0%		−2.6%
C—C bond		+14.8%	
Bond angle	−20.0° to +20.2°	−19.0° to +20.4°	−17.5° to +19.8°

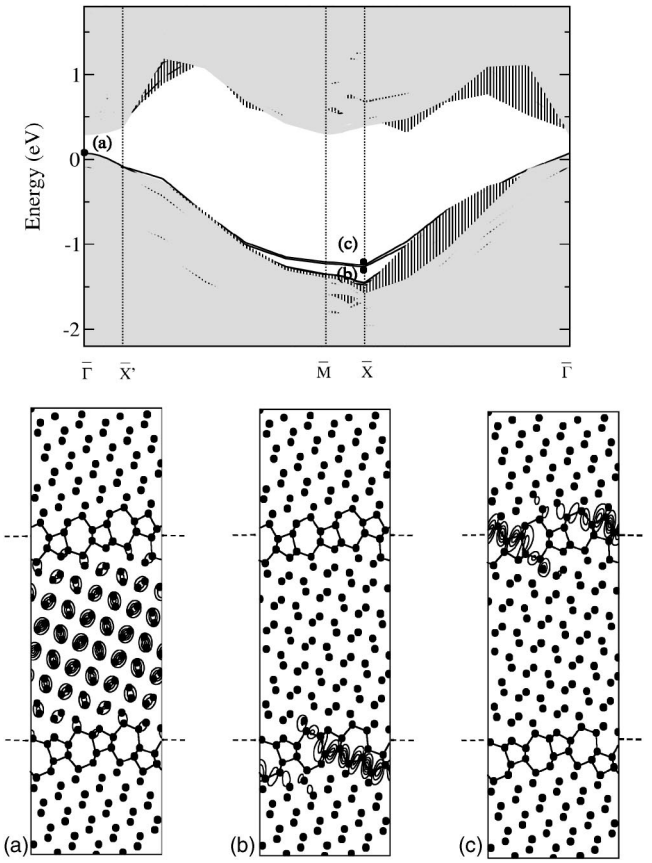

FIG. 13. Electronic band structure of the {115}/{$3\bar{3}02$} Si interface (upper panel). The projected bulk 3*C* and 2*H* band structures are presented as hatched or shaded regions. Wave-function squares of important states in the fundamental gap are also plotted (lower panel).

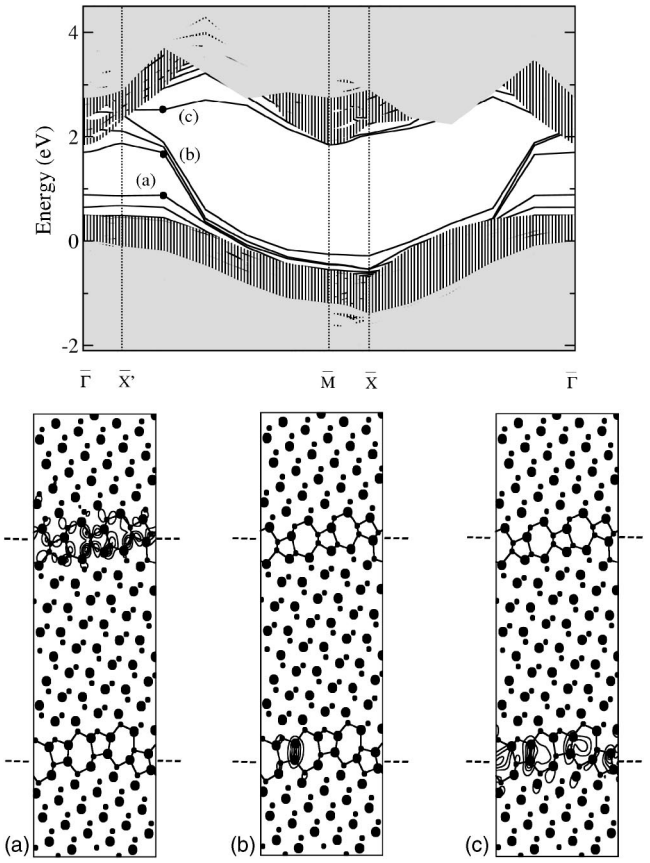

FIG. 14. Electronic band structure of C-rich and Si-rich {115}/{$3\bar{3}02$} interfaces in SiC (upper panel). The projected bulk 3*C* and 2*H* band structures are prevented as hatched or shaded regions. Wave-function squares of important states in the fundamental gap are also plotted (lower panel).

quantum wire presented in Fig. 1 will tend to have metallic properties in SiC.

IV. CONCLUSIONS

In this work, we have shown that first-principles calculations are able to predict the structural and electronic properties of extended two-dimensional defects. As examples we have examined three grain boundaries or internal interfaces in Si and SiC with cubic (diamond, zinc blende) or hexagonal (wurtzite) structure.

In the case of the {111}/{0001} interface between 3*C* and 2*H* polytypes, shallow states have been found close to the valence and conduction band edges of the ideal bulk structures. For SiC, in the limit of thin cubic inclusions in a hexagonal matrix, *ab initio* calculations are consistent with the results of a simple square well model corrected by the electric-field influence due to spontaneous polarization.

We have studied the effect of covalent or ionic bonds in the case of the $\Sigma 9\{221\}$ boundary between two tilted cubic crystals. Although this grain boundary is still tetrahedrally bonded, electronic states are generated in the fundamental gap. In Si, shallow states both above the VBM and below the CBM have been found. Whereas the states below the CBM are clearly identified as interface states, the states above the VBM have more the character of resonance states. In SiC, only states above the VBM have been found, with a strong localization at the odd-membered rings of the interfaces. The experimental observation of the interface in CVD deposited SiC films is justified by the low value of the interface energy which is of the order of the thermal energy.

We have presented calculations of the properties of the {115}/{$3\bar{3}02$} interface between cubic and hexagonal polytypes. While the interface system remains semiconducting in the case of Si, the presence of wrong Si—Si and C—C bonds in the case of SiC results in many interface bands with strong dispersion, making the system metallic.

ACKNOWLEDGMENTS

This work was financially supported by the EU Research and Training Network NANOPHASE (HPRN-CT-2000-00167).

*Current address: Laboratoire de Thermodynamique et Physico-Chimie Métallurgiques, Domaine Universitaire, BP 75, 38402 Saint-Martin-d'Hères Cedex, France.
†Electronic address: furth@ifto.uni-jena.de

[1] M. Y. Chou, M. L. Cohen, and S. G. Louie, Phys. Rev. B **32**, 7979 (1985).
[2] P. Käckell, J. Furthmüller, and F. Bechstedt, Phys. Rev. B **58**, 1326 (1998).
[3] C. Raffy, J. Furthmüller, and F. Bechstedt, Phys. Rev. B **66**, 075201 (2002).
[4] M. S. Miao, S. Limpijumnong, and W. R. L. Lambrecht, Appl. Phys. Lett. **79**, 4360 (2001).
[5] A. R. Verma and P. Krishna, *Polymorphism and Polytypism in Crystals* (Wiley, New York 1966).
[6] N. W. Jepps and T. F. Page, Prog. Cryst. Growth Charact. **7**, 259 (1983).
[7] O. L. Krivanek, S. Isoda, and K. Kobayashi, Philos. Mag. **36**, 931 (1977).
[8] O. L. Krivanek, Chem. Scr. **14**, 213 (1978).
[9] O. L. Krivanek and D. M. Maher, Appl. Phys. Lett. **32**, 451 (1978).
[10] M. Kohyama, Modell. Simul. Mater. Sci. Eng. **10**, R31 (2002).
[11] R. E. Thomson and D. J. Chadi, Phys. Rev. B **29**, 889 (1984).
[12] D. P. DiVincenzo, O. L. Alerhand, M. Schlüter, and J. W. Wilkins, Phys. Rev. Lett. **56**, 1925 (1986).
[13] J. Hornstra, Physica (Amsterdam) **25**, 409 (1959).
[14] C. R. M. Grovenor, J. Phys. C **18**, 4079 (1985).
[15] J. Q. Liu, M. Skowronski, C. Hallin, R. Söderholm, and H. Lendenmann, Appl. Phys. Lett. **80**, 749 (2002).
[16] H. Iwata, U. Lindefelt, S. Öberg, and P. R. Briddon, Phys. Rev. B **65**, 033203 (2001).
[17] M. Kohyama, Phys. Rev. B **65**, 184107 (2002).
[18] F. Bechstedt and P. Käckell, Phys. Rev. Lett. **75**, 2180 (1995).
[19] U. Starke, J. Schardt, J. Bernhardt, M. Franke, and K. Heinz, Phys. Rev. Lett. **82**, 2107 (1999).
[20] A. Fissel, U. Kaiser, B. Schröter, W. Richter, and F. Bechstedt, Appl. Surf. Sci. **184**, 37 (2001).
[21] F. Bechstedt, A. Fissel, U. Grossner, U. Kaiser, H.-C. Weissker, and W. Wesch, Mater. Sci. Forum **389–393**, 737 (2002).
[22] F. Bechstedt, A. Fissel, J. Furthmüller, U. Kaiser, H.-C. Weissker, and W. Wesch, Appl. Surf. Sci. **212–213**, 820 (2003).
[23] S. Bai, R. P. Devaty, W. J. Choyke, U. Kaiser, G. Wagner, and M. F. MacMillan, Appl. Phys. Lett. **83**, 3171 (2003).
[24] T. A. Arias and J. D. Joannopoulos, Phys. Rev. B **49**, 4525 (1994).
[25] M. Kohyama and R. Yamamoto, Phys. Rev. B **49**, 17 102 (1994); **50**, 8502 (1994).
[26] T. Y. Tan, H. Föll, and S. M. Hu, Philos. Mag. A **44**, 127 (1981).
[27] P. Pirouz, R. Chaim, and U. Dahmen, in *Defects in Electronic Materials*, edited by M. Stavola, S. J. Pearton, and G. Davies, Mater. Res. Soc. Symp. Proc. No. 104 (Materials Research Society, Pittsburgh, 1998), p. 133.
[28] P. Pirouz, R. Chaim, U. Dahmen, and K. H. Westmacott, Acta Metall. Mater. **38**, 313 (1990); U. Dahmen, K. H. Westmacott, P. Pirouz, and R. Chaim, *ibid.* **38**, 3273 (1990); P. Pirouz, U. Dahmen, K. H. Westmacott, and R. Chaim, *ibid.* **38**, 329 (1990).
[29] S. Q. Xiao and P. Pirouz, J. Mater. Res. **7**, 1406 (1992); P. Müllner and P. Pirouz, Mater. Sci. Eng., A **233**, 139 (1997).
[30] P. Hohenberg and W. Kohn, Phys. Rev. **136**, B864 (1964).
[31] W. Kohn and L. J. Sham, Phys. Rev. **140**, A1133 (1965).
[32] G. Kresse and J. Furthmüller, Comput. Mater. Sci. **6**, 15 (1996); Phys. Rev. B **54**, 11169 (1996).
[33] J. Furthmüller, P. Käckell, F. Bechstedt, and G. Kresse, Phys. Rev. B **61**, 4576 (2000).
[34] J. P. Perdew and A. Zunger, Phys. Rev. B **23**, 5048 (1981).
[35] H. J. Monkhorst and J. D. Pack, Phys. Rev. B **13**, 5188 (1976).
[36] R. Enderlein and N. J. M. Horing, *Fundamentals of Semiconductor Physics and Devices* (World Scientific, Singapore, 1997).
[37] P. Käckell and F. Bechstedt, Appl. Surf. Sci. **104/105**, 490 (1996).
[38] P. Käckell, B. Wenzien, and F. Bechstedt, Phys. Rev. B **50**, 17 037 (1994).
[39] C. Raffy, J. Furthmüller, and F. Bechstedt, J. Phys.: Condens. Matter **14**, 12 725 (2002).
[40] M. Murayama and T. Nakayama, Phys. Rev. B **49**, 4710 (1994).
[41] A. A. Stekolnikov, J. Furthmüller, and F. Bechstedt, Phys. Rev. B **65**, 115318 (2002).
[42] F. Bechstedt, A. Zywietz, K. Karch, B. Adolph, K. Tenelsen, and J. Furthmüller, Phys. Status Solidi B **202**, 35 (1997).
[43] H. Iwata, U. Lindefelt, S. Öberg, and P. R. Briddon, Mater. Sci. Forum **389–393**, 533 (2002); J. Appl. Phys. **93**, 1577 (2003).
[44] C. d'Anterroches and A. Bourret, Philos. Mag. A **49**, 783 (1984).
[45] A. Bourret, J. Phys. (Paris), Colloq. **46**, C4–27 (1985).
[46] K. C. Pandey, Phys. Rev. Lett. **47**, 1913 (1981).
[47] A. A. Stekolnikov, J. Furthmüller, and F. Bechstedt, Phys. Rev. B **65**, 115318 (2002).
[48] R. Biswas, R. M. Martin, R. J. Needs, and O. H. Nielsen, Phys. Rev. B **35**, 9559 (1987).
[49] K. Tanaka and M. Kohyama, Philos. Mag. A **82**, 215 (2002).
[50] E. Takuma and H. Ichinose, in *Influences of Interface and Dislocation Behavior on Microstructure Evolution*, edited by M. Aindow, M. D. Asta, M. V. Glazov, D. L. Medlin, A. D. Rollett, and M. Zaiser, Mater. Res. Soc. Symp. Proc. No. 652 (Materials Research Society, Warrendale, 2001), p. Y10.5.
[51] B. Cunningham, H. Strunk, and D. G. Ast, Appl. Phys. Lett. **40**, 237 (1982).
[52] J. D. Joannopoulos and M. L. Cohen, Phys. Rev. B **7**, 2644 (1973).
[53] S. Greulich-Weber, Phys. Status Solidi A **162**, 95 (1997).